

1

# An examination of the high-order dynamic interactions 2 underlying multi-dimensional timeseries data

3 Lucy L. W. Owen<sup>1</sup>, Thomas Hao Chang<sup>1,2</sup>, and Jeremy R. Manning<sup>1,†</sup>

<sup>1</sup>Department of Psychological and Brain Sciences,  
Dartmouth College, Hanover, NH

<sup>3</sup>Amazon.com, Seattle, WA

<sup>†</sup>Address correspondence to jeremy.r.manning@dartmouth.edu

4 March 22, 2019

5 **Abstract**

6 Most complex systems reflect dynamic interactions between myriad evolving components (e.g., interacting  
7 molecules, interacting brain systems, interacting individuals within a social network or ecological  
8 system, coordinated components within a mechanical or digital device, etc.). Despite that these interactions  
9 are central to the full system’s behavior (e.g., removing a component from the full system can change the  
10 entire system’s behavior), dynamic interactions cannot typically be directly measured. Rather, the interactions  
11 must be inferred through their hypothesized role in guiding the dynamics of system components.  
12 Here we use a model-based approach to inferring dynamic interactions from timeseries data. In addition  
13 to examining first-order interactions (e.g., between pairs of components) we also examine higher-order  
14 interactions (e.g., that characterize mirrored structure in the patterns of interaction dynamics displayed  
15 by different subsets of components). We apply our approach to two datasets. First, we use a synthetic  
16 dataset, for which the underlying dynamic interactions are known, to show that our model recovers those  
17 ground-truth dynamic interactions. We also apply our model to a neuroimaging dataset and show that the  
18 high-order dynamic interactions exhibited by brain data vary meaningfully as a function of the cognitive  
19 “richness” of the stimulus people are experiencing.

20 **Introduction**

21 The dynamics of the observable universe are meaningful in three respects. First, the behaviors of the *atomic*  
22 *units* that exhibit those dynamics are highly interrelated. The actions of one unit typically have implications  
23 for one or more other units. In other words, there is non-trivial *correlational structure* defining how different  
24 units interact with and relate to each other. Second, that correlational structure is *hierarchical* in the sense  
25 that it exists on many spatiotemporal scales. The way one group of units interacts may relate to how another  
26 group of units interact, and the interactions between those groups may exhibit some rich structure. Third,  
27 the structure at each level of this correlational hierarchy changes from moment to moment, reflecting the  
28 “behavior” of the full system.

29 These three properties (rich correlations, hierarchical organization, and dynamics) are major hallmarks  
30 of many complex systems. For example, within a single cell, the cellular components interact at many

31 spatiotemporal scales, and those interactions change according to what that single cell is doing. Within a  
32 single human brain, the individual neurons interact within each brain structure, and the structures interact  
33 to form complex networks. The interactions at each scale vary according to the functions our brains are  
34 carrying out. And within social groups, interactions at different scales (e.g., between individuals, family  
35 units, communities, etc.) vary over time according to changing goals and external constraints.

36 Although many systems exhibit rich dynamic correlations at many scales, a major challenge to studying  
37 such patterns is that typically neither the correlations nor the hierarchical organizations of those correlations  
38 may be directly observed. Rather, these fundamental properties must be inferred indirectly by examining  
39 the observable parts of the system— e.g., the behaviors of the individual atomic units of that system. In  
40 the *Methods* section, we propose a series of mathematical operations that may be used to recover dynamic  
41 correlations at a range of scales (i.e., orders of interaction). In the *Results* section, we demonstrate how our  
42 approach may be applied to multi-dimensional timeseries data: a synthetic dataset where the underlying  
43 dynamic correlations are known (we use this dataset to validate our approach), and a neuroimaging dataset  
44 comprising data collected as participants listened to a story (Simony et al., 2016). In different experimental  
45 conditions in the neuroimaging study, participants listened to altered versions of the story that varied in  
46 cognitive richness: the intact story (fully engaging), a scrambled version of the story where the paragraphs  
47 were presented in a randomized order (moderately engaging), a second scrambled condition where the  
48 words were presented in a random order (minimally engaging), and a “rest” condition where the participants  
49 did not listen to any version of the story (control condition). We use the neuroimaging dataset to examine  
50 how higher-order structure in brain data varies as a function of the cognitive richness of the stimulus.

## 51 Methods

52 There are two basic steps to our approach (Fig. 2). In the first step, we take a number-of-timepoints ( $T$ ) by  
53 number-of-features ( $F$ ) *matrix of observations* ( $\mathbf{X}$ ) and we return a  $T$  by  $\frac{F^2-F}{2}$  *matrix of dynamic correlations* ( $\mathbf{Y}$ ).  
54 Here  $\mathbf{Y}_0$  describes, at each moment, how all of the features (columns of  $\mathbf{X}$ ) are inferred to be interacting.  
55 (Since the interactions are assumed to be non-recurrent and symmetric, only the upper triangle of the full  
56 correlation matrix is computed.) In the second step, we project  $\mathbf{Y}_0$  onto an  $F$ -dimensional space, resulting in  
57 a new  $T$  by  $F$  matrix  $\mathbf{Y}_1$ . Note that  $\mathbf{Y}_1$  contains information about the correlation dynamics present in  $\mathbf{X}$ , but  
58 represented in a compressed number of dimensions. By repeatedly applying these two steps in sequence,  
59 we can examine and explore higher order dynamic correlations in  $\mathbf{X}$ .

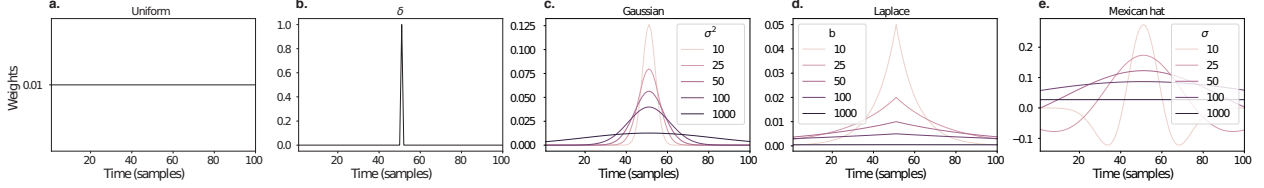


Figure 1: **Examples of time-varying weights.** Each panel displays per-timepoint weights at  $t = 50$ , evaluated for 100 timepoints (1, ..., 100). **a. Uniform weights.** The weights are timepoint-invariant; observations at all timepoints are weighted equally, and do not change as a function of  $t$ . This is a special case of weight function that reduces dynamic correlations to static correlations. **b. Dirac delta function.** Only the observation at timepoint  $t$  is given weight (of 1), and weights for observations at all other timepoints are set to 0. **c. Gaussian weights.** Each observation's weights fall off in time according to a Gaussian probability density function centered on  $\mu = t$ . Weights derived using several different example variance parameters ( $\sigma^2$ ) are displayed. **d. Laplace weights.** Each observation's weights fall off in time according to a Laplace probability density function centered on  $\mu = t$ . Weights derived using several different example scale parameters ( $b$ ) are displayed. **e. Mexican hat (Ricker wavelet) weights.** Each observation's weights fall off in time according to a Ricker wavelet centered on  $t$ . This function highlights the *contrasts* between local versus surrounding activity patterns in estimating dynamic correlations. Weights derived using several different example width parameters ( $\sigma$ ) are displayed.

## 60 Dynamic correlations

Given a matrix of observations, we can compute the (static) correlations between any pair of observations,  $\mathbf{X}_i$  and  $\mathbf{X}_j$  using:

$$\text{corr}(\mathbf{X}_i, \mathbf{X}_j) = \frac{\sum_{t=1}^T (\mathbf{X}_i(t) - \bar{\mathbf{X}}_i)(\mathbf{X}_j(t) - \bar{\mathbf{X}}_j)}{\sqrt{\sum_{t=1}^T \sigma_{\mathbf{X}_i}^2 \sigma_{\mathbf{X}_j}^2}}, \text{ where} \quad (1)$$

$$\bar{\mathbf{X}}_k = \sum_{t=1}^T \mathbf{X}_k(t), \text{ and} \quad (2)$$

$$\sigma_{\mathbf{X}_k}^2 = \sum_{t=1}^T (\mathbf{X}_k(t) - \bar{\mathbf{X}}_k)^2 \quad (3)$$

61     We can generalize this formula to compute time-varying correlations by incorporating a *weight function*  
62     that takes a time  $t$  as input, and returns how much the observed data every timepoint (including  $t$ ) contribute  
63     to the correlations at time  $t$  (Fig. 1).

Given a weight function  $w(t)$  for timepoint  $t$ , evaluated at timepoints in the interval  $[1, \dots, T]$ , we can

extend the static correlation formula in Equation 2 to reflect an *instantaneous correlation* at timepoint  $t$ :

$$\text{timecorr}(\mathbf{X}_i, \mathbf{X}_j, t) = \frac{\sum_{t=1}^T (\mathbf{X}_i(t) - \tilde{\mathbf{X}}_i(t))(\mathbf{X}_j(t) - \tilde{\mathbf{X}}_j(t))}{\sqrt{\sum_{t=1}^T \tilde{\sigma}_{\mathbf{X}_i}^2(t) \tilde{\sigma}_{\mathbf{X}_j}^2(t)}}, \text{ where} \quad (4)$$

$$\tilde{\mathbf{X}}_k(t) = \sum_{i=1}^T w(t, i) \mathbf{X}_k(i), \quad (5)$$

$$\tilde{\sigma}_{\mathbf{X}_k}^2(t) = \sum_{i=1}^T (\mathbf{X}_k(i) - \tilde{\mathbf{X}}_k(t))^2, \quad (6)$$

- and  $w(t, i)$  is shorthand for  $w(t)$  evaluated at timepoint  $i$ . Equation 5 may be used to estimate the instantaneous correlations between every pair of observations, at each timepoint (i.e.,  $\mathbf{Y}$ ).

## 66 Inter-subject dynamic correlations

Equation 5 provides a means of taking a single observation matrix,  $\mathbf{X}$  and estimating the dynamic correlations from moment to moment,  $\mathbf{Y}$ . Suppose that one has access to a set of multiple observation matrices that reflect the same phenomenon. For example, one might collect neuroimaging data from several experimental participants, as each participant performs the same task (or sequence of tasks). Let  $\{\mathbf{X}_1, \mathbf{X}_2, \dots, \mathbf{X}_P\}$  reflect the  $T$  by  $F$  observation matrices for each of  $P$  participants in an experiment. We can use *inter-subject functional connectivity* (ISFC; Simony et al., 2016) to compute the degree of stimulus-driven correlations reflected in the multi-participant dataset at a given timepoint  $t$  using:

$$\bar{\mathbf{C}}(t) = M \left( R \left( \frac{1}{2P} \sum_{i=1}^P Z(Y_i(t))^T + Z(Y_i(t)) \right) \right), \quad (7)$$

where  $M$  extracts and vectorizes the diagonal and upper triangle of a symmetric matrix,  $Z$  is the Fisher  $z$ -transformation (Zar, 2010):

$$Z(r) = \frac{\log(1+r) - \log(1-r)}{2} \quad (8)$$

$R$  is the inverse of  $Z$ :

$$R(z) = \frac{\exp(2z-1)}{\exp(2z+1)}, \quad (9)$$

and  $\mathbf{Y}_i(t)$  denotes the correlation matrix (Eqn. 2) between each column of  $\mathbf{X}_i$  and each column of the average observations from all *other* participants,  $\bar{\mathbf{X}}_{\setminus i}$ :

$$\bar{\mathbf{X}}_{\setminus i} = R \left( \frac{1}{P-1} \sum_{i \in \setminus i} Z(\mathbf{X}_i) \right), \quad (10)$$

where  $\setminus i$  denotes the set of all participants other than participant  $i$ . In this way, the  $T$  by  $\left(\frac{F^2-F}{2} + F\right)$  matrix  $\bar{\mathbf{C}}$  is the time-varying extension of the ISFC approach developed by Simony et al. (2016).

## 69 Higher-order correlations

Given a timeseries of dynamic correlations (e.g., obtained using Eqn. 5), higher-order correlations reflect the dynamic correlations between columns of  $\mathbf{Y}$ . Given unlimited computing resources, one could use repeated applications of Equation 5 to estimate these higher-order correlations (i.e., substituting in the previous output,  $\mathbf{Y}$ , for the input,  $\mathbf{X}$  in the equation). However, because each output  $\mathbf{Y}$  has  $O(F^2)$  columns relative to  $F$  columns in the input  $\mathbf{X}$ , the output of Equation 5 grows with the square of the number of repeated applications (total cost of computing  $n^{\text{th}}$  order correlations is  $O(F^{2n})$  for  $n \in \mathcal{J}, n > 0$ ). When  $F$  or  $n$  is large, this approach quickly becomes intractable.

To make progress in computing  $\mathbf{Y}_{n+1}$ , we can approximate  $\mathbf{Y}_n$  by computing an  $O(F)$ -dimensional embedding of  $\mathbf{Y}_n$ , termed  $\hat{\mathbf{Y}}_n$ , and then we can apply Equation 5 to  $\hat{\mathbf{Y}}_n$  rather than directly to  $\mathbf{Y}_n$ . This enables us to maintain  $O(n)$  scaling with respect to  $n$ , rather than exponential scaling via the direct approach.

There are many possible methods for computing  $\hat{\mathbf{Y}}_n$  from  $\mathbf{Y}_n$ , including traditional dimensionality reduction approaches and graph theory based approaches as described next. In the *Discussion* section we elaborate on other potential approaches.

## 83 Dimensionality reduction-based approaches to computing $\hat{\mathbf{Y}}_n$

Commonly used dimensionality reduction algorithms include Principal Components Analysis (PCA; Pearson, 1901), Probabilistic PCA (PPCA; Tipping & Bishop, 1999), Exploratory Factor Analysis (EFA; Spearman, 1904), Independent Components Analysis (ICA; Jutten & Herault, 1991; Comon et al., 1991),  $t$ -Stochastic Neighbor Embedding ( $t$ -SNE; van der Maaten & Hinton, 2008), Uniform Manifold Approximation and Projection (UMAP; McInnes & Healy, 2018), non-negative matrix factorization (NMF; Lee & Seung, 1999), Topographic Factor Analysis (TFA) Manning et al. (2014), Hierarchical Topographic Factor analysis (HTFA) Manning et al. (2018), Topographic Latent Source Analysis (TLSA) Gershman et al. (2011), Dictionary learning (J. B. Mairal et al., 2009; J. Mairal et al., 2009), deep autoencoders (Hinton & Salakhutdinov,

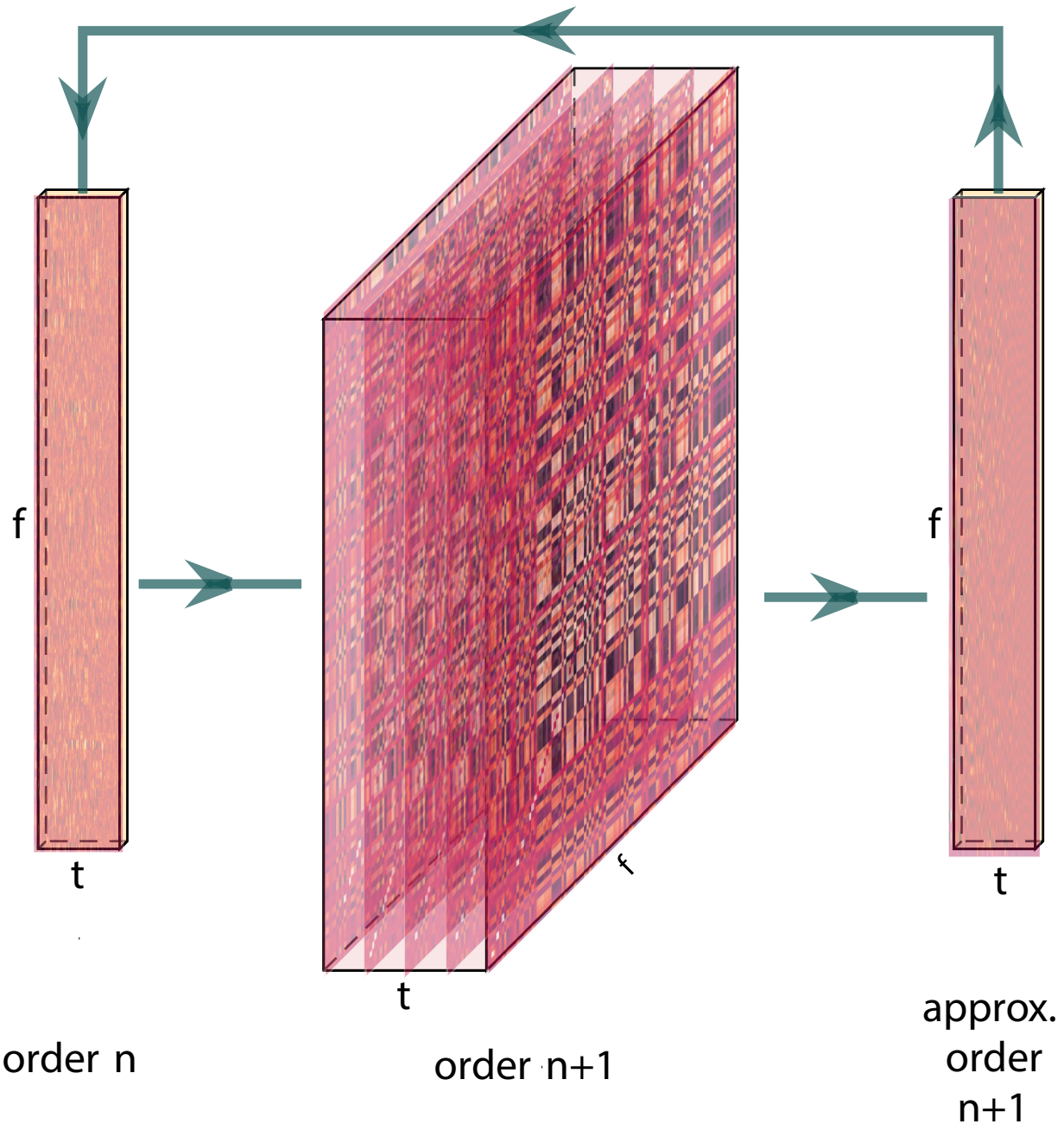


Figure 2: **Computing higher order correlations.** Correlations are computed then approximated to the same size as original data. This process is repeated to computer

92 among others. While complete characterizations of each of these algorithms is beyond the scope of  
93 the present manuscript, the general intuition driving these approaches is to compute the  $\hat{\mathbf{Y}}$  with  $i$  columns  
94 that is closest to the original  $\mathbf{Y}$  with  $j$  columns, and where (typically)  $i \ll j$ . The different approaches place  
95 different constraints on what properties  $\hat{\mathbf{Y}}$  must satisfy and which aspects of the data are compared (and  
96 how) to characterize the match between  $\hat{\mathbf{Y}}$  and  $\mathbf{Y}$ .

97 Applying dimensionality reduction algorithms to  $\mathbf{Y}$  yields a  $\hat{\mathbf{Y}}$  whose columns reflect weighted combi-  
98 nations (or nonlinear transformations) of the original columns of  $\mathbf{Y}$ . This has two main consequences. First,  
99 with each repeated dimensionality reduction, the resulting  $\hat{\mathbf{Y}}_n$  has lower and lower fidelity (with respect to  
100 what the “true”  $\mathbf{Y}_n$  might have looked like without using dimensionality reduction to maintain scalability).  
101 In other words, computing  $\hat{\mathbf{Y}}_n$  is a lossy operation. Second, whereas the columns of  $\mathbf{Y}_n$  may be mapped  
102 directly onto pairs of columns of  $\mathbf{Y}_{n-1}$ , that mapping either becomes less cleanly defined in  $\hat{\mathbf{Y}}_n$  due to the  
103 reweightings and/or nonlinear transformations.

104 **Graph theory-based approaches to computing  $\hat{\mathbf{Y}}_n$**

105 Graph theoretic measures take as input a matrix of interactions (e.g., using the above notation, an  $F \times F$   
106 correlation matrix or binarized correlation matrix reconstituted from a single timepoint’s row of  $\mathbf{Y}$ ) and  
107 return as output a set of  $F$  measures describing how each node (feature) sits within that interactions matrix  
108 with respect to the rest of the population. Common measures include betweenness centrality (the proportion  
109 of shortest paths between each pair of nodes in the population that involves the given node in question; e.g.,  
110 Newman, 2005; Opsahl et al., 2010; Barthélemy, 2004; Geisberger et al., 2008; Freeman, 1977); diversity and  
111 dissimilarity (characterizations of how differently connected a given node is from others in the population;  
112 e.g., Rao, 1982; Lin, 2009; Ricotta & Szeidl, 2006); Eigenvector centrality and pagerank centrality (measures of  
113 how influential a given node is within the broader network; e.g., Newman, 2008; Bonacich, 2007; Lohmann  
114 et al., 2010; Halu et al., 2013); transfer entropy and flow coefficients (a measure of how much information is  
115 flowing from a given node to other nodes in the network; e.g., Honey et al., 2007; Schreiber, 2000);  $k$ -coreness  
116 centrality (a measure of the connectivity of a node within its local sub-graph; e.g., Alvarez-Hamelin et al.,  
117 2005; Christakis & Fowler, 2010); within-module degree (a measure of how many connections a node has to  
118 its close neighbors in the network; e.g., Rubinov & Sporns, 2010); participation coefficient (a measure of the  
119 diversity of a node’s connections to different sub-graphs in the network; e.g., Rubinov & Sporns, 2010); and  
120 sub-graph centrality (a measure of a node’s participation in all of the network’s sub-graphs; e.g., Estrada &  
121 Rodríguez-Velázquez, 2005).

122 As an alternative to the above dimensionality reduction approach to embedding  $\mathbf{Y}_n$  in a lower-dimensional

space, but still allowing for scalable explorations of higher-order structure in the data, we also explore using the above graph theoretic measures as a means of obtaining  $\hat{\mathbf{Y}}_n$ . In particular: for a given graph theoretic measure,  $\eta : \mathcal{R}^{F \times F} \rightarrow \mathcal{R}^F$ , we can use  $\eta$  to transform each row of  $\mathbf{Y}_n$  in a way that characterizes the corresponding graph-theoretic properties of each column. Whereas the dimensionality reduction approach to computing  $\hat{\mathbf{Y}}_n$  is lossy, the graph-theory approach is lossless. However, whereas the dimensionality reduction approach maintains ties (direct or indirect) to the original activity patterns reflected in  $\mathbf{Y}_{n-1}$ , the graph-theory approach does not. Instead, the graph-theory characterizes the nature and timecourse of each feature's *participation* in the network.

### 131 **Evaluation metrics**

132 We evaluate our approach to extracting dynamic correlations and higher-order correlations using several  
133 metrics detailed next. First, we generated synthetic data using known time-varying correlations, and then  
134 we evaluated the fidelity with which Equation 5 could recover those correlations (for synthetic datasets  
135 with different properties, and using different kernels to define the weights; Fig. 1). We then turned to a  
136 series of analyses on a (real) neuroimaging dataset where the ground truth correlations were *not* known.  
137 We evaluated whether the recovered correlations could be used to accurately label held-out neuroimaging  
138 data with the time at which it was collected, and also whether the history of correlations (and higher-order  
139 correlations) from time 0 to  $t - 1$  could be used to predict future activity patterns at time  $t$ . We used these  
140 latter evaluations (using timepoint decoding and predictions of held-out future data) as a proxy for gauging  
141 how much explanatory power the recovered correlations held with respect to the observed data.

### 142 **Generating synthetic data**

143 Ramping dataset and block dataset. Add details (Fig. ??)

### 144 **Recovery of ground truth parameters from synthetic data**

145 Apply timecorr with a given kernel, then correlate each recovered correlation matrix with the ground truth.  
146 Explore how recovery varies with the kernel, kernel parameters, and specific structure of the data (e.g. slow  
147 changes as in the ramping dataset, versus rapid changes as in the block dataset).

### 148 **Timepoint decoding**

149 To explore how higher-order structure varies with stimulus structure and complexity, we used a previous  
150 neuroimaging dataset Simony et al. (2016) in which participants listened to an audio recording of a story;

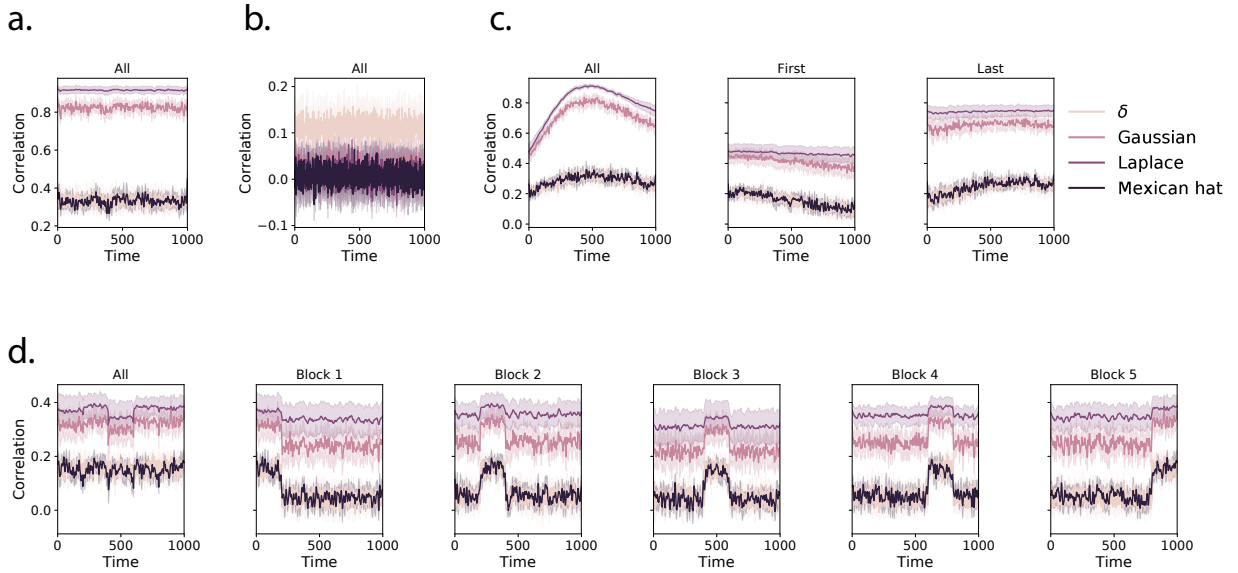


**Figure 3: Dynamic correlation recovery with synthetic data.** **a.** Recovery using a constant dataset. Using constant dataset, how well can we recover using different kernels. **b.** Recovery using random dataset. **c.** Ramping recovery. **d.** Block recovery

151 36 participants listen to an intact version of the story, 17 participants listen to time-scrambled recordings of  
 152 the same story where paragraphs were scrambled, 36 participants listen to word-scrambled version and 36  
 153 participants lay in rest condition.

154 Prior work has shown participants share similar neural responses to richly structured stimuli when  
 155 compared to stimuli with less structure. To assess whether the moment-by-moment higher order correlations  
 156 were reliably preserved across participants, we used inter-subject functional connectivity (ISFC) to isolate  
 157 the time-varying correlational structure (functional connectivity patterns that were specifically driven by  
 158 the story participants listened to. Following the analyses conducted by (HTFA) Manning et al. (2018), we  
 159 first applied *hierarchical topographic factor analysis* (HTFA) to the fMRI datasets to obtain a time series of  
 160 700 node activities for every participant. We then computed the dynamic weighted ISFC using a gaussian  
 161 kernel with a width of 5. We then approximated these dynamic correlation using PCA and computed the  
 162 dynamic weighted ISFC on the approximations. We repeated this process up to 10th order approximated  
 163 correlations.

164 To assess decoding accuracy, we randomly divided participants for each stimulus into training and  
 165 testing groups. For the zeroth order, we computed the mean factor activity for each group. For all  
 166 subsequent orders up to the tenth order, we computed the mean approximated dynamic ISFC of factor  
 167 activity for each group. For each group of participants in turn, we compared these activity patterns (using  
 168 Pearson correlations) to estimate the story times each pattern corresponded to.

169 Specifically, we asked, for each timepoint: what are the correlations between the first group's and second  
170 group's activity patterns at each order. We then took weighted mixture of the correlation matrices at each  
171 order using mixing parameter,  $\phi$ , where  $0 < \phi < 1$  reflects a weighted mixture of order based decoding. We  
172 optimized  $\phi$ , by subdividing the training group. We note that the decoding test we used is a conservative  
173 in which we count a timepoint label as incorrect if it is not an exact match.

## 174 Results

### 175 Synthetic data

176 Figure: overall timecourse of recovery, also recovery near event boundaries.

### 177 Neuroimaging dataset (Simony et al., 2016)

178 Figures: decoding by level For our decoding analysis, we used HTFA-derived node activities Manning et  
179 al. (2018) from fMRI data collected as participants listened to an audio recording of a story (intact condition;  
180 36 participants), listened to time scrambled recordings of the same story (17 participants in the paragraph-  
181 scrambled condition listened to the paragraphs in a randomized order and 36 in the word-scrambled  
182 condition listened to the words in a randomized order), or lay resting with their eyes open in the scanner  
183 (rest condition; 36 participants). We sought to demonstrate how higher-order correlations may be used to  
184 examine dynamic interactions of brain patterns in (real) multi-subject fMRI datasets. This story listening  
185 dataset was collected as part of a separate study, where the full imaging parameters, image preprocessing  
186 methods, and experimental details may be found (Simony et al., 2016). The dataset is available at <http://arks.princeton.edu/ark:/88435/dsp015d86p269k>.

188 We next evaluated if our model of high-order correlations in brain activity can capture cognitively  
189 relevant brain patterns. We performed a decoding analysis, using cross validation to estimate (using other  
190 participants' data) which parts of the story each weighted-mixture of higher-order brain activity pattern  
191 corresponded to (see *Materials and methods*). We note that our primary goal was not to achieve perfect  
192 decoding accuracy, but rather to use decoding accuracy as a benchmark for assessing whether different  
193 neural features specifically capture cognitively relevant brain patterns.

194 Separately for each experimental condition, we divided participants into two groups. For the zeroth  
195 order, we computed the mean factor activity for each group. For all subsequent orders up to the tenth  
196 order, we computed the mean approximated dynamic ISFC of factor activity for each group (see *Materials*  
197 and *methods*). For each order, we correlated the group 1 activity patterns with group 2 activity patterns.

198 We then subdivided the group 1 to obtain an optimal weighting parameter for each order's correlation  
199 matrix using the same cross validation method. We used the optimal weighting parameters to obtain a  
200 weighted-mixture of each order's correlation matrix. Using these correlations, we labeled the group 1  
201 timepoints using the group 2 timepoints with which they were most highly correlated; we then computed  
202 the proportion of correctly labeled group 1 timepoints. (We also performed the symmetric analysis whereby  
203 we labeled the group 2 timepoints using the group 1 timepoints as a template.) We repeated this procedure  
204 10 times (randomly re-assigning participants to the two groups each time) to obtain a distribution of  
205 decoding accuracies for each experimental condition. (There were 272 timepoints for paragraph condition,  
206 300 timepoints for intact and word conditions, and 400 timepoints for rest condition, so chance performance  
207 on this decoding test is was  $\frac{1}{272}$ ,  $\frac{1}{300}$ , and  $\frac{1}{400}$  respectively.

## 208 Discussion

- 209 • multiple timescale representations (a la Hasson group) implies first-order network interactions.  
210 higher-order interactions imply generalizations between interacting representations (e.g. mirrored  
211 schema, a la Norman/Baldassano/Hasson). possibly cite NTB 2013 science review, using as evidence  
212 that this is where the field is going (voxels → patterns (L0) → interactions (L1) → higher order patterns  
213 (L2+)).
- 214 • related approaches: sliding window, phase-based correlations, within-ROI spatial correlations at each  
215 timepoint, granger causality, other explit models (e.g. virtual brain).
- 216 • other applications: molecular interactions (protein folding?), diagnosis (e.g. psychiatric disorders  
217 as network flow problems- gratton work?), social network dynamics (e.g. financial markets, social  
218 media interactions)

## 219 Concluding remarks

220 the universe is complicated and we need scalable approaches to studying how the pieces are interacting to  
221 make sense of it. one small step for mankind, and so on.

## 222 Acknowledgements

223 We acknowledge discussions with Luke Chang, Hany Farid, Paxton Fitzpatrick, Andrew Heusser, Eshin  
224 Jolly, Qiang Liu, Matthijs van der Meer, Judith Mildner, Gina Notaro, Stephen Satterthwaite, Emily Whitaker,

225 Weizhen Xie, and Kirsten Ziman. Our work was supported in part by NSF EPSCoR Award Number 1632738  
226 to J.R.M. and by a sub-award of DARPA RAM Cooperative Agreement N66001-14-2-4-032 to J.R.M. The  
227 content is solely the responsibility of the authors and does not necessarily represent the official views of our  
228 supporting organizations.

## 229 Author contributions

230 Concept: J.R.M. Implementation: T.H.C., L.L.W.O., and J.R.M. Analyses: L.L.W.O and J.R.M.

## 231 References

- 232 Alvarez-Hamelin, I., Dall'Asta, L., Barrat, A., & Vespignani, A. (2005). *k*-corr decomposition: a tool for the  
233 visualiztion of large scale networks. *arXiv*, cs/0504107v2.
- 234 Barthélemy, M. (2004). Betweenness centrality in large complex networks. *European Physical Journal B*, 38,  
235 163–168.
- 236 Bonacich, P. (2007). Some unique properties of eigenvector centrality. *Social Networks*, 29(4), 555–564.
- 237 Christakis, N. A., & Fowler, J. H. (2010). Social network sensors for early detection of contagious outbreaks.  
238 *PLoS One*, 5(9), e12948.
- 239 Comon, P., Jutten, C., & Herault, J. (1991). Blind separation of sources, part II: Problems statement. *Signal  
240 Processing*, 24(1), 11 - 20.
- 241 Estrada, E., & Rodríguez-Velázquez, J. A. (2005). Subgraph centrality in complex networks. *Physical Review  
242 E*, 71(5), 056103.
- 243 Freeman, L. C. (1977). A set of measures of centrality based on betweenness. *Sociometry*, 40(1), 35–41.
- 244 Geisberger, R., Sanders, P., & Schultes, D. (2008). Better approximation of betweenness centrality. *Proceedings  
245 of the meeting on Algorithm Engineering and Experiments*, 90–100.
- 246 Gershman, S., Blei, D., Pereira, F., & Norman, K. (2011). A topographic latent source model for fMRI data.  
247 *NeuroImage*, 57, 89–100.
- 248 Halu, A., Mondragón, R. J., Panzarasa, P., & Bianconi, G. (2013). Multiplex PageRank. *PLoS One*, 8(10),  
249 e78293.

- 250 Hinton, G. E., & Salakhutdinov, R. R. (2006). Reducing the dimensionality of data with neural networks.  
251 *Science*, 313(5786), 504–507.
- 252 Honey, C. J., Kötter, R., Breakspear, M., & Sporns, O. (2007). Network structure of cerebral cortex shapes  
253 functional connectivity on multiple time scales. *Proceedings of the National Academy of Science USA*, 104(24),  
254 10240–10245.
- 255 Jutten, C., & Herault, J. (1991). Blind separation of sources, part I: An adaptive algorithm based on  
256 neuromimetic architecture. *Signal Processing*, 24(1), 1–10.
- 257 Lee, D. D., & Seung, H. S. (1999). Learning the parts of objects by non-negative matrix factorization. *Nature*,  
258 401, 788–791.
- 259 Lin, J. (2009). Divergence measures based on the Shannon entropy. *IEEE Transactions on Information Theory*,  
260 37(1), 145–151.
- 261 Lohmann, G., Margulies, D. S., Horstmann, A., Pleger, B., Lepsien, J., Goldhahn, D., … Turner, R. (2010).  
262 Eigenvector centrality mapping for analyzing connectivity patterns in fMRI data of the human brain.  
263 *PLoS One*, 5(4), e10232.
- 264 Mairal, J., Ponce, J., Sapiro, G., Zisserman, A., & Bach, F. R. (2009). Supervised dictionary learning. *Advances  
265 in Neural Information Processing Systems*, 1033–1040.
- 266 Mairal, J. B., Bach, F., Ponce, J., & Sapiro, G. (2009). Online dictionary learning for sparse coding. *Proceedings  
267 of the 26th annual international conference on machine learning*, 689–696.
- 268 Manning, J. R., Ranganath, R., Norman, K. A., & Blei, D. M. (2014). Topographic factor analysis: a Bayesian  
269 model for inferring brain networks from neural data. *PLoS One*, 9(5), e94914.
- 270 Manning, J. R., Zhu, X., Willke, T. L., Ranganath, R., Stachenfeld, K., Hasson, U., … Norman, K. A. (2018).  
271 A probabilistic approach to discovering dynamic full-brain functional connectivity patterns. *NeuroImage*,  
272 180, 243–252.
- 273 McInnes, L., & Healy, J. (2018). t-SNE: Uniform manifold approximation and projection for dimension  
274 reduction. *arXiv*, 1802(03426).
- 275 Newman, M. E. J. (2005). A measure of betweenness centrality based on random walks. *Social Networks*, 27,  
276 39–54.
- 277 Newman, M. E. J. (2008). The mathematics of networks. *The New Palgrave Encyclopedia of Economics*, 2, 1–12.

- 278 Opsahl, T., Agneessens, F., & Skvoretz, J. (2010). Node centrality in weighted networks: generalizing degree  
279 and shortest paths. *Social Networks*, 32, 245–251.
- 280 Pearson, K. (1901). On lines and planes of closest fit to systems of points in space. *The London, Edinburgh,  
281 and Dublin Philosophical Magazine and Journal of Science*, 2, 559-572.
- 282 Rao, C. R. (1982). Diversity and dissimilarity coefficients: a unified approach. *Theoretical Population Biology*,  
283 21(1), 24–43.
- 284 Ricotta, C., & Szeidl, L. (2006). Towards a unifying approach to diversity measures: Bridging the gap  
285 between the Shannon entropy and Rao's quadratic index. *Theoretical Population Biology*, 70(3), 237–243.
- 286 Rubinov, M., & Sporns, O. (2010). Complex network measures of brain connectivity: uses and interpreta-  
287 tions. *NeuroImage*, 52, 1059–1069.
- 288 Schreiber, T. (2000). Measuring information transfer. *Physical Review Letters*, 85(2), 461–464.
- 289 Simony, E., Honey, C. J., Chen, J., & Hasson, U. (2016). Uncovering stimulus-locked network dynamics  
290 during narrative comprehension. *Nature Communications*, 7(12141), 1–13.
- 291 Spearman, C. (1904). General intelligence, objectively determined and measured. *American Journal of  
292 Psychology*, 15, 201–292.
- 293 Tipping, M. E., & Bishop, C. M. (1999). Probabilistic principal component analysis. *Journal of Royal Statistical  
294 Society, Series B*, 61(3), 611–622.
- 295 van der Maaten, L. J. P., & Hinton, G. E. (2008). Visualizing high-dimensional data using t-SNE. *Journal of  
296 Machine Learning Research*, 9, 2579-2605.
- 297 Zar, J. H. (2010). *Biostatistical analysis*. Prentice-Hall/Pearson.